Impact of model uncertainties on the fatigue reliability of offshore wind turbines

Jan-Tore Horn[a,b,*], Jørgen R. Krokstad[b], Bernt J. Leira[b]

[a] *Centre for Autonomous Marine Operations and Systems (NTNU AMOS), NTNU, Trondheim, Norway*
[b] *Department of Marine Technology, NTNU, Trondheim, Norway*

Abstract

The impact of environmental load uncertainties on the spatial fatigue reliability of offshore wind turbine foundations is discussed and exemplified. Design procedures are utilizing overall or partial safety factors to include different model- and statistical uncertainties. Uncertainties in the final design are related to decisions taken during the design process, such as; load models, analysis methods and statistical descriptions. Furthermore, to benefit from more elaborate methods, strategies to account for reduced uncertainties by increased knowledge must be adopted. This is especially important for the offshore wind energy industry, where the aim is to produce renewable energy at a competitive cost level. The challenges and consequences of using a detailed design basis are exemplified and discussed through structural reliability analyses. Epistemic load effect uncertainties related to the foundation fatigue will be presented for a detailed wind directional model, wind-wave misalignment, and a second order wave load model. It will be shown that all of these represent important uncertainties to consider during the fatigue design of an offshore wind farm.

Keywords: Offshore wind turbines; reliability; fatigue; misalignment; wave loads; uncertainties; directions

---

1. Introduction

It is important to be aware of design conservatism and lack of knowledge as the offshore wind energy industry is expanding with an increasing number of offshore farms. Several rules and regulations, e.g. [1, 2, 3], have been developed in order to mitigate the risk involved in construction, transport, installation and operation of offshore wind turbines.

Increased accuracy in modelling the environmental loads may both increase and decrease the long term load effects determining the survivability of the structure. For instance, it was demonstrated in [4] that separating between wind sea and swell was beneficial with respect to the foundation fatigue. On the other hand, more detailed wave

*Corresponding author
Email address: `jan-tore.horn@ntnu.no` (Jan-Tore Horn)

load models may increase loads, and hence the risk of failure, as seen in e.g. [5, 6, 7, 8]. It is then expected that methods beyond state-of-the-art will introduce over-conservatism unless the safety factors are re-calibrated for detailed time-domain analyses.

Safety factors found in guidelines and literature are to be used in combinations with characteristic values of their respective load effects. For instance, the characteristic SN-curve used in fatigue design is defined as the mean value minus two standard deviations [9], in order to ensure conservatism. Then, a characteristic fatigue damage can be found whose value is increased with a design fatigue factor (DFF) to obtain the governing fatigue result. However, safety factors do not consider the dynamic characteristics of the structure in combination with the accuracy of the engineering load models. In other words, a more accurate method, giving higher load amplitudes (or stress ranges), is not automatically rewarded with a lower safety factor.

In order to bypass the use of general safety factors, probabilistic analyses can be performed to document a sufficient level of structural safety. Probabilistic fatigue limit state (FLS) analyses are performed using long term response statistics in combination with uncertainties related to the engineering models, which are accounted for by stochastic variables in the structural reliability analyses (SRA). Relevant literature on general SRA can be found in e.g. [10, 11], where [10] has a relatively pragmatic approach suitable for new readers. In [12], an overview of probabilistic design of wind turbines is presented, including uncertainties related to environmental models and stress calculation. Load effect uncertainties can be a function of available in-situ measurements, as presented in [13]. Further, given a set of load effect- and model uncertainties, safety factors for a given level of reliability can be calculated as demonstrated in e.g. [14].

Uncertainties related to design of offshore wind turbines, may be divided into aleatory and epistemic (see e.g. [15, 16]). Aleatory, or statistical, uncertainties include variation due to the stochastic nature of the wind and wave loading. This include both long-term variation related to temporal weather changes and the short-term randomness of wave elevation and wind gusts. A significant amount of computational efforts to cover all environmental combinations during the 20-25 years of operational lifetime may be required. Second, epistemic, or systematic, uncertainties are related to the engineering models. Here, these are defined as the physical models of and the statistical models of the environmental processes. These uncertainties can be mitigated with high-fidelity models of the physical processes, but also in terms of access to extensive in-situ measurements of the metocean parameters to fit accurate statistical models demonstrated in e.g. [17].

The paper is structured as follows: first, the environmental and numerical model is briefly presented. Second, a model for the spatial fatigue damage used in the reliability analysis is presented. Finally, some cases with increased model accuracies are compared to a state-of-the-art base case analysis to illustrate how the foundation reliability is affected.

2. Environment

Hindcast data for description of the wind and wave environment is provided by the Norwegian Meteorological Institute and the NORA10 database [18] for Dogger Bank. The data contains information about the wind speed, wind direction and significant wave height, peak period, and directions. The data is valid for periods of 3 hour durations and contains information for the previous 60 years. Some of the available parameters are listed in Tab. 1. The amount of available data is sufficient for providing an accurate statistical description of the weather at the chosen site. Discussions regarding the statistical uncertainty of the environment can be found in e.g. [17]. These aleatory uncertainties are not accounted for in this paper, and the environmental model is assumed to reflect the true environment. The environmental joint distribution is then modelled as:

$$f_{\mathbf{X}_e} = f_{\Theta_v} \cdot f_{V|\Theta_v} \cdot f_{H_S|V} \cdot f_{T_P|H_S} \cdot f_{\Theta_r} \tag{1}$$

Details on the the distribution types are given in Tab. 1, but the reader is referred to [17] for details regarding construction of the conditional model, where good resemblance with the hindcast data is demonstrated. Note that the wind-wave misalignment Θ_r, is de-coupled from the wind speed and significant wave height, for simplicity. As seen in [17], this is a reasonable assumption for the site in question. It can be explained by the dynamics of wind direction changes and the inherent inertia of the misalignment angle, which is present for all wind-wave conditions.

Table 1: Marginal distribution types and description of environmental parameters

Parameter		Distribution	Description	Unit
V	v	2-p Weibull	Wind speed at 100 meters	[m/s]
Θ_v	θ_v	von Mises mix	Wind direction at 100 meters	[deg]
H_S	h	3-p Weibull	Significant wave height for wind sea	[m]
T_P	t	Lognormal	Peak period for wind sea spectrum	[m]
Θ_r	θ	Normal	Relative wind-wave direction	[deg]

3. Numerical model

The numerical model represents a bottom-fixed monopile-mounted turbine with tower and rotor-nacelle assembly as described in [19]. The dimensions of the monopile and transition piece can be found in Fig. 1. To maintain a realistic natural period while increasing the overall height of the structure, the tower thickness is increased by 20% [20]. The resulting first fore-aft and side-to-side natural periods are approximately 4.4 seconds, while the periods related to the second vibrational model are about 0.9 seconds in both directions. Consequently, the system is stiff, but still subjected to significant dynamic response from both wind and waves. The controller is an extended version of [21] with the possibility of increasing the fore-aft aerodynamic damping and avoid rotational speeds coinciding with the natural periods of the system. For integration in time-domain and calculation of aerodynamic loads, the finite-element method (FEM) code USFOS/vpOne is used [22, 23, 24], while the hydrodynamic loads are calculated by an external Matlab/Octave routine and imported to the FEM code. The turbulent wind field is created with TurbSim [25] using the Kaimal spectrum and a turbulence intensity of 10%. For a parked/idling turbine, the blades are pitched to 82 degrees relative to the rotor plane, inducing only a slow rotation of the rotor. All fatigue damage results are based on the bending stresses at the mudline for this model.

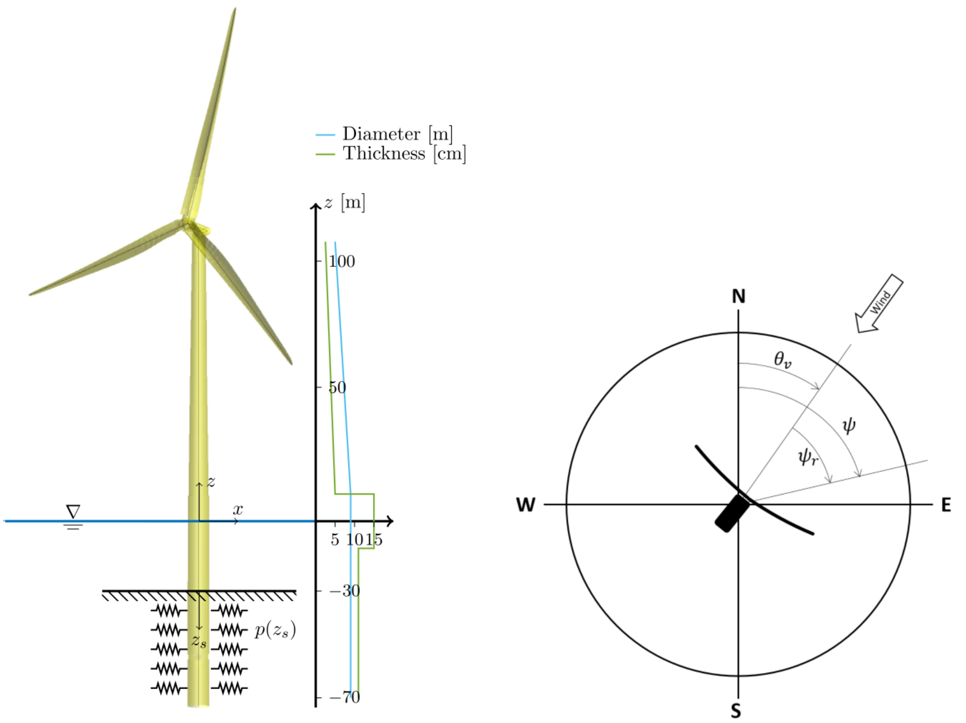

(a) Numerical model with dimensions

(b) Definition of wind direction and location on pile, absolute (ψ) and relative (ψ_r)

Figure 1: Numerical wind turbine model geometry

4. Fatigue limit state

In this section, a novel method for the spatial fatigue reliability of a monopile foundation is presented. The method utilizes the fact that the current foundation is radially symmetric, and assumes uniform soil conditions in all directions.

The failure function for fatigue at a location ψ along the pile circumference, after n years in service is:

$$g(\psi) = \Delta - n\left[\alpha\, d_{op}(\psi) + (1-\alpha)\, d_{id}(\psi)\right] \tag{2}$$

where α is the fraction of the time of which the wind turbine is operational, d_{op} and d_{id} is the expected yearly fatigue damage accumulation for an operational and idling turbine, respectively. Furthermore, Δ is the maximum allowable utilization of the material fatigue life, including uncertainties related to the Palmgren-Miner summation of stress cycles. The probability of failure can then be found by evaluating

$$p_f = P[g \leq 0] \tag{3}$$

by some appropriate reliability method, such as the first- or second order reliability method (FORM/SORM), or Monte Carlo simulations (MCS) [11]. The corresponding reliability index is $\beta = -\Phi^{-1}(p_f)$, where Φ^{-1} is the inverse standard normal cumulative density function (CDF).

The fact that the current wind turbine is considered to be rotationally symmetric, means that one only needs to perform simulations for a single direction, and superposition the results according to the relative direction: $\psi_r = \psi - \theta_v$. Hence the fatigue damage at ψ can be found as:

$$d(\psi) = \int_v \int_{\theta_v} d(\psi_r|v)\, f_{V,\Theta_v}(v, \theta_v)\, d\theta_v\, dv \tag{4}$$

where $d(\psi_r|v)$ is the fatigue damage during operation or idling at ψ_r given the wind speed v. The total fatigue damage is then found by integrating over all wind speeds and directions along with the probability density function f_{V,Θ_v}. Further, is can be shown that the fatigue damage can be expressed in terms of a closed form solution as [26, 27]:

$$\begin{aligned} d(\psi_r|v) =& \nu\, T \left\{ \frac{[\, a\, X_M\, X_L\, (t/t_{\text{ref}})^k\,]^{m_1}}{K_1} \Gamma \left[1 + \frac{m_1}{b}, \left(\frac{\Delta\sigma_0}{a} \right)^b \right] \right. \\ & \left. + \frac{[\, a\, X_M\, X_L\, (t/t_{\text{ref}})^k\,]^{m_2}}{K_2} \gamma \left[1 + \frac{m_2}{b}, \left(\frac{\Delta\sigma_0}{a} \right)^b \right] \right\} \end{aligned} \tag{5}$$

when the stress range is Weibull distributed with scale parameter $a = a(\psi_r, v)$ and shape parameter $b = b(\psi_r, v)$. The remaining parameters are; average number of stress cycles $\nu = \nu(\psi_r, v)$, pile thickness t, stress calculation uncertainty in the numerical model X_M, and load effect uncertainty X_L. Furthermore, $\Delta\sigma_0$, K_i and m_i are material parameters related to the SN-curve, and k and t_{ref} are parameters to account for actual plate thickness. All parameters are listed in Tab. 1. The stress range distribution includes uncertainties related to the significant wave height and peak period for a given wind speed, which is found by evaluating

$$\Delta\sigma(\psi_r, v) = \int_h \int_t \Delta\sigma(\psi_r, v|h, t)\, f_{H_S,T_P}(h, t)\, dt\, dh \tag{6}$$

using Monte Carlo simulations until the scale and shape parameters (a and b) for each wind speed has met the convergence criteria, a coefficient-of-variance (CoV) less than 0.05 is chosen in this case. An example of statistical uncertainty related to the number of simulations can be found in e.g. [28] when using a response surface method. As a result, there are some statistical uncertainties related to the Weibull parameters, which are neglected in the present study to limit the scope. Example Weibull fits are shown in Fig. 2, where a 2-parameter Weibull distribution is fitted to the distribution tail using two fitting points in the upper range of the data. It was observed that the fatigue damage error computed using the fitted Weibull stress range and direct evaluation of the Palmgren-Miner was less than 5% in all cases. For fatigue calculations, it is important that the stress range representation is correct for the stress ranges contributing the most to the total fatigue. As indicated in Fig. 3, the fatigue damage derived from approximately $\Delta\sigma > 10$ [MPa] or $\log \Delta\sigma > 2.3$ is dominating, meaning that the Weibull fit should be accurate in this range. Also, note that there is a very small contribution from the low-cycle part of the SN-curve ($\Delta\sigma > \Delta\sigma_0$). It is assumed that the 2-parameter

Weibull with tail weighting is sufficient in all present cases to satisfy this requirement, although a 3-parameter Weibull may yield even more accurate results. The advantage with 2-parameter Weibull is the closed-form solution to the Palmgren-Miner summation as presented in Eq. (5).

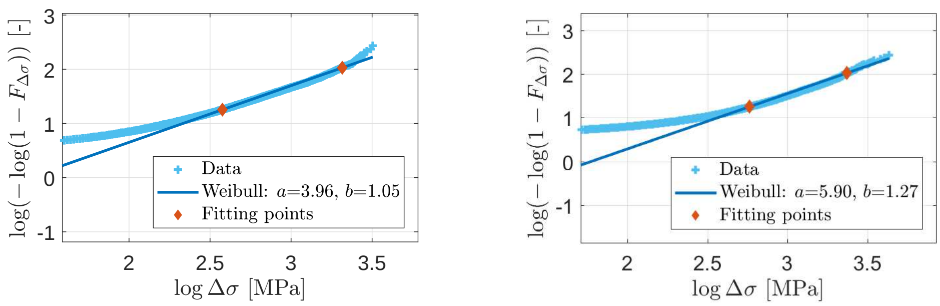

(a) Wind speed of 14m/s and misalignment angle of 0 degrees

(b) Wind speed of 20m/s and misalignment angle of -40 degrees

Figure 2: Example stress range distributions with Weibull fits in the tail, for the critical location on the pile circumference for operational turbine

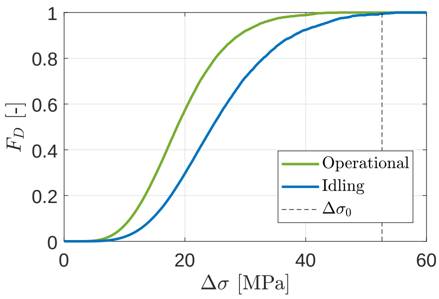

Figure 3: Cumulative fatigue damage contribution from stress ranges for an operational and idling turbine. The stress limit Δs_0 for the two-slope SN-curve is shown.

The scale and shape parameters are then found as a function of wind speed and relative pile location as shown in Fig. 4 and 5 for operational and idling turbine, respectively. It is suggested that an exponential response surface is used:

$$a(\psi_r, v) = \frac{\exp(p_0 + p_1\, v + p_2\, v^2)}{1 + p_3\,(v - v_0)^2} \cdot (\cos 2\psi_r + 1) + \exp(p_4 + p_5\, v) \tag{7}$$

for a and the ratio a/b with fitting parameters $p_{0,\ldots,5}$ and a dominating wind speed v_0 to account for additional excitation at the wind speed where resonance is most likely. The fitting function is strictly positive, differentiable, and periodic with respect to relative location ψ_r. It was proven to be well-suited for representing the Weibull parameters of the stress ranges as function of wind speed and relative pile location. Final fitting constants can be found in Tab. 3. Note that a similar expression will not be used for the zero-crossing frequency ν, which will be treated as an independent variable due to relatively small changes in terms of V and ψ_r. Instead, the zero-crossing frequency for operational (ν_{op}) and idling (ν_{id}) turbine can be found in Tab. 2, derived from Fig. 4c and 5c, respectively. The procedure for obtaining the response surface in the (v, ψ_r)-domain is summed up in the flowchart in Fig. 6.

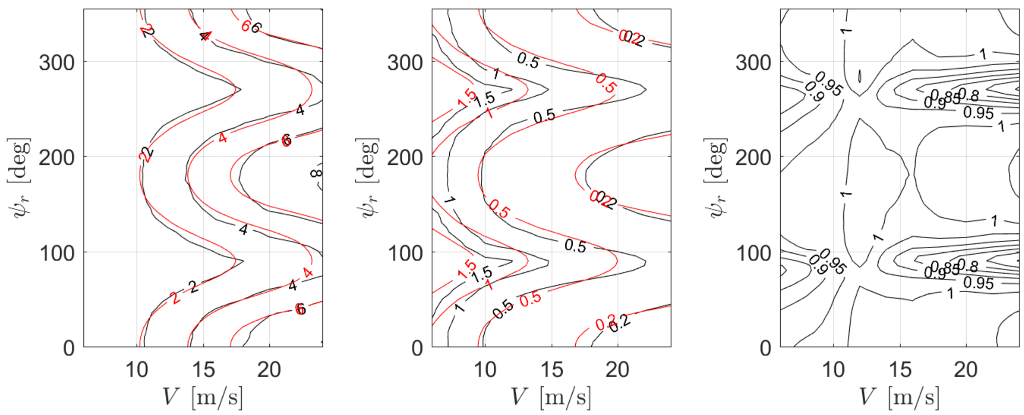

(a) $a(\psi_r, v)$ (b) $b(\psi_r, v)/a(\psi_r, v)$ (c) $\nu(\psi_r, v)$

Figure 4: Response contours for operational turbine in co-directional sea. Result from MCS in the full environmental domain by Eq. (6) in black and periodic surface fit in red.

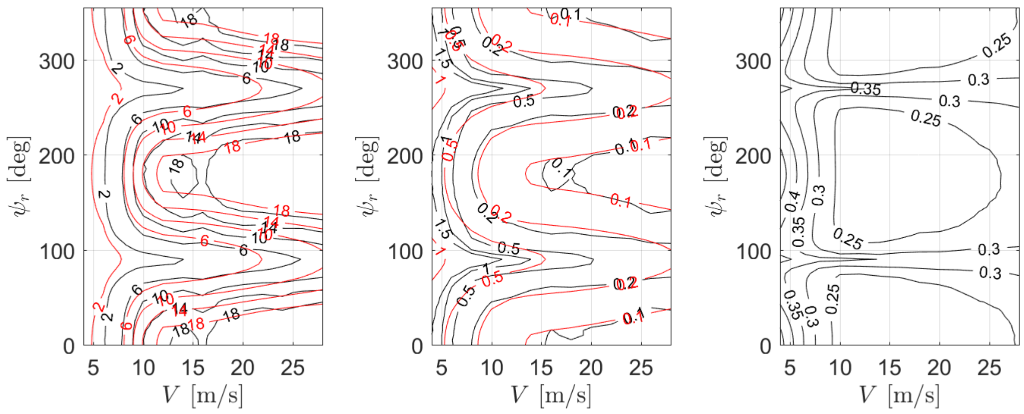

(a) $a(\psi_r, v)$ (b) $b(\psi_r, v)/a(\psi_r, v)$ (c) $\nu(\psi_r, v)$

Figure 5: Response contours for idle turbine in co-directional sea. Result from MCS in the full environmental domain by Eq. (6) in black and surface fit in red.

Variable	Distribution	Expected value	Standard deviation
Δ	Lognormal	1	0.3
α	Beta	0.94	0.04
$\Delta\sigma_0$	Fixed	52.63	-
m_1	Fixed	3	-
m_2	Fixed	5	-
$\log K_1$	Normal	12.164	0.2
$\log K_2$	Normal	16.106	0.2
X_M	Lognormal	1.0	0.1
$X_{L,a}$	Lognormal	1.0	0.03
$X_{L,h}$	Fixed	1.0	-
ν_{id}	Lognormal	0.27	0.05
ν_{op}	Lognormal	0.96	0.06
t	Fixed	0.11	-
t_{ref}	Fixed	0.025	-
k	Fixed	0.2	-

Table 2: Stochastic variables for the base case probabilistic analysis in FLS.

Table 3: Fitting constants

Turbine state	Parameter	p_0	p_1	p_2	p_3	p_4	p_5	v_0
Operational	a	-5.12	0.600	-1.51	0.00	-1.42	0.121	10
Operational	a/b	-3.09	0.370	-0.890	0.00	-1.36	0.103	10
Idling	a	-3.0	0.57	-0.94	0.12	0.083	0.078	10
Idling	a/b	-1.5	0.29	-0.34	0.036	-0.37	0.069	10

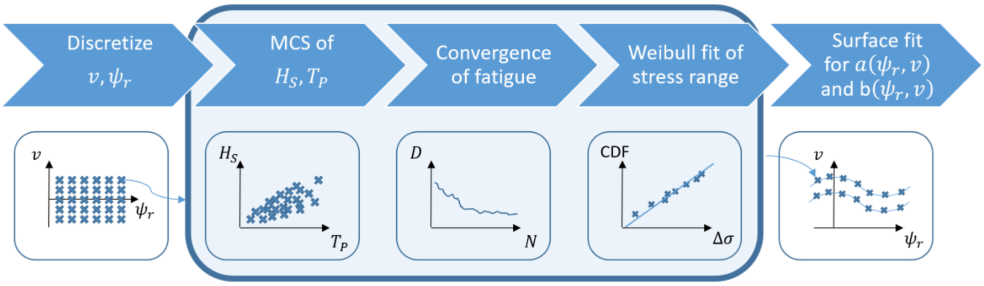

Figure 6: Steps to obtain the response surface used in the present fatigue reliability methodology

5. Case studies

115 Three case studies will be presented with respect to the impact on fatigue reliability; wind directional model, wind-wave misalignment and wave load effect.

5.1. Base case

The base case contains the uncertainties in Tab. 2, no wind-wave misalignment, linear wave theory, and independent wind speed and direction:

$$f_{V,\Theta_v} = f_V \cdot f_{\Theta_v} \tag{8}$$

5.2. Uncertainty in wind speed and -direction

When modelling the joint wind speed and wind direction, two approaches are possible as illustrated in Fig. 7. Either the Weibull parameters describing the wind speed distribution is dependent on the wind direction as in Fig. 7a, or the wind directional distribution is dependent on the wind speed as illustrated in Fig. 7b. The latter description is elaborated on in [17]. For the present case, the wind speed distribution is modelled as dependent on the direction, so that:

$$f_{V,\Theta_v} = f_{V|\Theta_v} \cdot f_{\Theta_v} \tag{9}$$

Hence, the Fourier fit of the scale and shape parameter as shown in Fig. 7a is used, combined with the marginal wind directional distribution, which is the red curve in Fig. 7b.

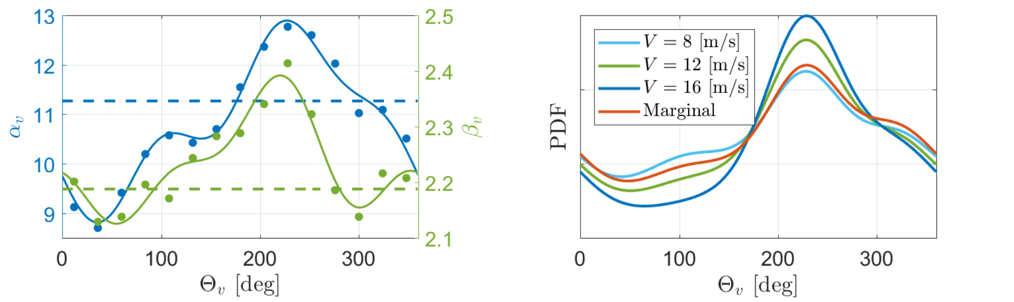

(a) Wind speed Weibull parameters as function of wind direction with Fourier fit (solid), compared to marginal values (dashed)

(b) Wind directional distribution for different wind speeds using a mixed von Mises distribution [17].

Figure 7: Dependency between wind speed and wind direction

The effect on the reliability when solving Eq. (3) using Monte Carlo simulations (MCS) is shown in Fig. 8. It is clear that the wind directional model does not affect the average reliability on the pile circumference, but since high wind speeds are more likely to originate from the south-west, a fatigue damage concentration is found at approximately $\psi = 50$ and $\psi = 230$ degrees. The difference from the base case at $\psi = 230$ corresponds to about 2 years of operational lifetime, meaning that the fatigue life calculated using decoupled wind speed and direction is non-conservative. Consequently, one must consider the multi-directionality of the metocean conditions as required in [3], but also with the distribution parameters as functions of the wind direction. Otherwise, an additional safety factor should be applied, calibrated to approximately $1 + 2/25 = 1.08$ in this specific case.

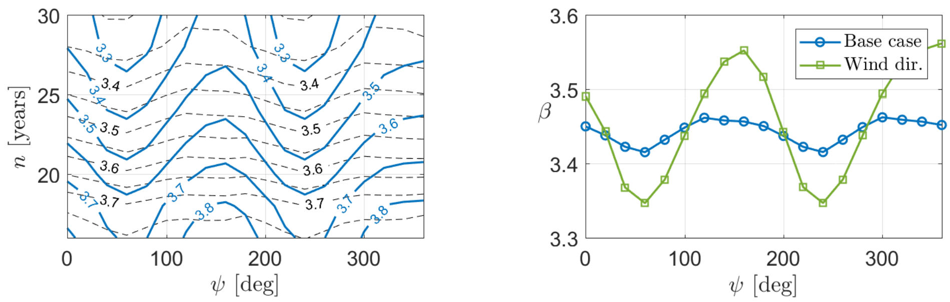

(a) Reliability index as function of years in operation and location on pile. Base case in dashed for comparison.

(b) Reliability index for 25 years in operation

Figure 8: Effect on reliability index when introducing dependency between wind speed and direction.

5.3. Uncertainty in the load effect induced by misalignment

Here, the fatigue damage uncertainty, or reliability, due to the wind-wave misalignment is presented. As illustrated in Fig. 9a, the fatigue damage increases approximately with the square of the misalignment angle. Interestingly, the effect is larger to one side due to the directionally dependent damping induced by the rotation of the rotor [4]. In Fig. 9b, the fatigue damage is weighted according to the probability of occurrence, described by the marginal distribution of wind speed and misalignment angle. Not surprisingly, misalignment will contribute significantly to the estimated fatigue, as we also can see from the reliability estimate later on.

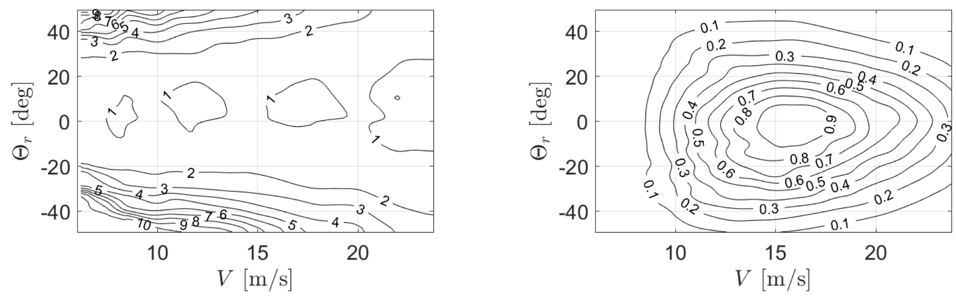

(a) Contours of fatigue normalized for each wind speed

(b) Contours of fatigue damage weighted according to joint probability of wind speed and misalignment angle

Figure 9: Effect of misalignment on the maximum fatigue damage around the pile circumference.

To account for the effect of wind-wave misalignment on the stress range along the pile circumference, some corrections are made to Eq. (7):

$$
\begin{aligned}
a_{mis}(\psi_r, v, \theta_r) = & \frac{\exp(p_0 + p_1\, v + p_2\, v^2)}{1 + p_3\,(v - v_0)^2} \cdot (\gamma_a(v, \theta_r)\, \cos 2(\psi_r - \psi_r^c) + 1) \\
& + \gamma_c(v, \theta_r)\, \exp(p_4 + p_5\, v)
\end{aligned}
\tag{10}
$$

where ψ_r^c is the phase-shift of the most critical fatigue damage location on the pile due to increasing transverse motions. A regression analysis is shown in Fig. 10b, which includes all wind speeds. Note that as the misalignment angle increases, the location accumulating the most fatigue damage is shifting even further, meaning that the turbine is vibrating more sideways than what is expected when only considering the misalignment angle. Furthermore, γ_a is to correct for the amplitude increase ($d_M - d_m$) as illustrated in Fig. 10a, and γ_c is accounting for the increase in average fatigue, μ_d. There are more differences than change in amplitude and mean value, which are neglected in this study to keep Eq. (10) fairly simple. A two-step procedure is performed for the fitting procedure, to obtain a reasonable fit with limited data. First, Eq. (7) is fitted for the zero-misalignment cases. Second, the corrections to the stress amplitude and mean are fitted to the following equation:

$$
\gamma(v, \theta_r) = p_1\, \sin^{p_2}(\theta_r - p_3) + 1 \tag{11}
$$

which is periodic, with maximum value for $\theta_r = p_3 + \pi/2$. In this case, a total of 100 10-minute simulations are performed for each combination of v and θ_r, including variations in H_S and T_P by Eq. (6). The resulting parameters can be found in Tab. 4 as functions of the wind speed.

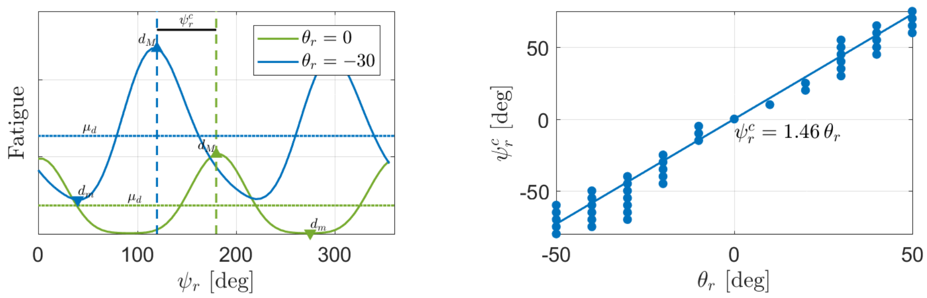

(a) Circumferential fatigue distribution for a single wind speed for two different misalignment angles. The means (μ_d), peaks (d_M), troughs (d_m) and angular correction (ψ_r^c) is shown.

(b) Correlation between misalignment angle and the circumferential location of maximum fatigue damage with fitted linear regression function

Figure 10: Effects of wind-wave misalignment

Table 4: Misalignment correction parameters as function of wind speed

Parameter	p_1	p_2	p_3
γ_a	$3.24\,\exp(-0.069\,v)$	4	$1.09\,\exp(0.085\,v)$
γ_c	$1.84\,\exp(-0.062\,v)$	2	$1.75\,\exp(0.067\,v)$

The results in Fig. 11 show that the misalignment is a significant contributor to the foundation reliability with the present formulations. Figure 11a, shows that a turbine subjected to misalignment conditions during its lifetime, will have an expected lifetime of approximately 7 years less compared to a turbine only operating in co-directional sea. In Fig. 11b, the circumferential fatigue reliability after 25 years in operation is shown, indicating a significant change in the reliability index when accounting for misalignment, both in magnitude and how the fatigue distributes over the circumference.

From this study, a partial safety factor can be derived regarding uncertainty in load effects from misalignment. Assuming that the base case represents a design fatigue analysis, and a reliability index of 3.4 is the reference for 25 years, a case-specific partial safety factor of $1 + 7/25 = 1.28$ must be applied to the case with co-directional sea to reflect the increased fatigue accumulation.

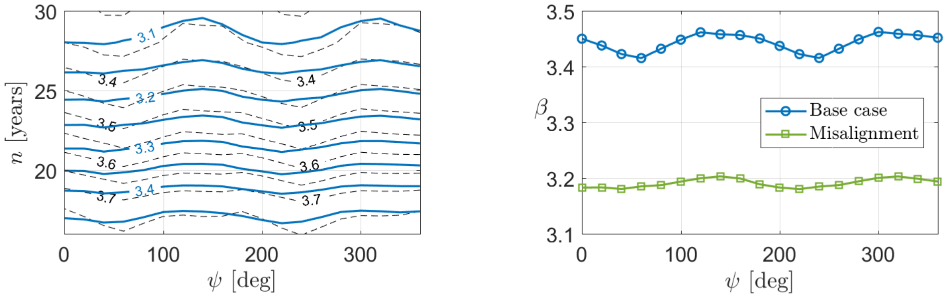

(a) Reliability index as function of years in operation and location on pile. Base case in dashed.

(b) Reliability index for 25 years in operation

Figure 11: Effect of misalignment on the foundation fatigue reliability index.

5.4. Uncertainty in wave loads

The final case study is related to the impact of higher order wave loads on the fatigue of the foundation. Several previous studies have concluded that second or higher order loads will have little impact on the design fatigue in the foundation and tower, see e.g. [5, 6]. While others show that non-linear loads can potentially reduce the lifetime significantly [29, 30]. This section studies the structural reliability impact of a second order load model compared to linear wave loads on the foundation fatigue damage.

In [31], investigations were made on the fatigue sensitivity to wave kinematics models and coefficients in the Morison equation [32] used for applying the wave loads. Further, [33] performed a sensitivity study on the fatigue where the MacCamy and Fuchs [34] load model was used to account for linear diffraction, including a frequently used second order kinematics model [35, 36] without any correction for diffraction forces. The studies are limited to a few sea states and little variation in the significant wave height and peak period for each wind speed. To the authors knowledge, no comprehensive studies have been performed accounting for the statistical uncertainty of the steepness of the sea state for a given wind speed, which is important for the magnitude of the higher order loading [37]. Also, no previous study has included the second order diffraction terms in relation to the wave load uncertainty, which may be of importance, depending on the size of the monopile [38], damping level and the modal shapes of the structure.

Here, the panel code Wamit is used for generating wave loads. For first order loads, the resulting pressure on the foundation can be found with:

$$p^{(1)}(z,t) = \mathcal{R}\left\{ \sum_j \zeta_{a,j} \sum_i n_{x,i}\, A_i\, p^{(1)}_{i,j}(z)\, e^{i\omega_j\, t - i\epsilon_j} \right\} \tag{12}$$

where $p_{i,j}$ represent the pressure at panel i due the the excitation frequency ω_j. Furthermore, A_i is the panel area, $n_{x,i}$ is the vector normal to the panel, and $\zeta_{a,j}$ is the wave amplitude corresponding to frequency ω_j, generated using the JONSWAP spectrum with default peak shape parameter [39]. The first order loads are calculated to the mean surface and no surface effects from wave elevation is present. The outer summation can be evaluated efficiently by using an inverse fast Fourier transform (FFT) [40]. For the second order sum-frequency force, a similar approach is used. The pressure due to sum-frequency components is then:

$$p^{+}(z,t) = \mathcal{R}\left\{ \sum_{k}\sum_{j} \zeta_{a,j}\, \zeta_{a,k} \sum_{i} n_{x,i}\, A_i\, p^{+}_{i,j,k}(z)\, e^{i(\omega_j+\omega_k)\,t}\, e^{-i(\epsilon_j+\epsilon_k)} \right\} \tag{13}$$

where the two outer summations can be evaluated efficiently with a two-dimensional inverse FFT as in e.g. [41]. The second order pressure is then found as:

$$p(z) = \begin{cases} p^{(1)}(z) + p^{+}(z) & \text{if } -h < z \leq 0 \\ p^{(1)}(0) & \text{if } 0 < z \leq \eta \end{cases} \tag{14}$$

for the first order surface elevation η. The horizontal force is then consistent to the second order, including the second order contribution from the surface elevation (see e.q. [6]).

In order to estimate the impact of uncertainty of wave-induced load effects on the foundation fatigue, the uncertainty introduced in the stress range in the foundation must be assessed. This is done in a similar manner as in [29], finding the load effect uncertainty as the ratio of the damage equivalent loads (DEL) between identical runs with non-linear and linear wave load model. The DEL is taken as the fatigue damage obtained from the rainflow-counted stress range at the mudline for zero misalignment $\Delta\sigma_y$. It is expected that this is a conservative measure for the load effect uncertainty on the pile circumference. Note that no further changes are made to the response surface presented in Section 4. After simplifying the expression by removing constant material parameters, the wave load uncertainty can be expressed as:

$$X_{L,h} = \frac{\left(\frac{1}{N}\sum_{i=1}^{N} \Delta\sigma_{y,NL,i}^{m_2}\right)^{1/m_2}}{\left(\frac{1}{N}\sum_{i=1}^{N} \Delta\sigma_{y,L,i}^{m_2}\right)^{1/m_2}} \tag{15}$$

where NL denotes non-linear loads with sum-frequency panel pressures and L is linear wave loading. Furthermore, $m_2 = 5$ is the material parameter for the high-cycle part of the SN-curve, which is dominating in this case. Due to significant aerodynamic damping from the large rotor during operation (demonstrated in [4]) and interaction between aerodynamic and hydrodynamic load effects, the load effect uncertainty must be found for operational and idling states of the turbine separately. Due to the higher possibility of transient responses during the low damped state for an idling turbine, the load effect uncertainty is larger for an idling turbine. In Fig. 12, the wave load effect uncertainty for an operational turbine is visualized as a function of H_S and T_P using the expected wind speed, while the uncertainty for an idling turbine is found in Fig. 13. By utilizing the statistical dependency between wind speed, significant wave height and peak period, the wave load effect uncertainty is re-sampled to a function of wind speed only, which is given in Fig. 14. Clearly, the uncertainty increases for an idling turbine. The functions given in Fig. 14 replaces the default mean and standard deviation of $X_{L,h}$ in Tab. 2.

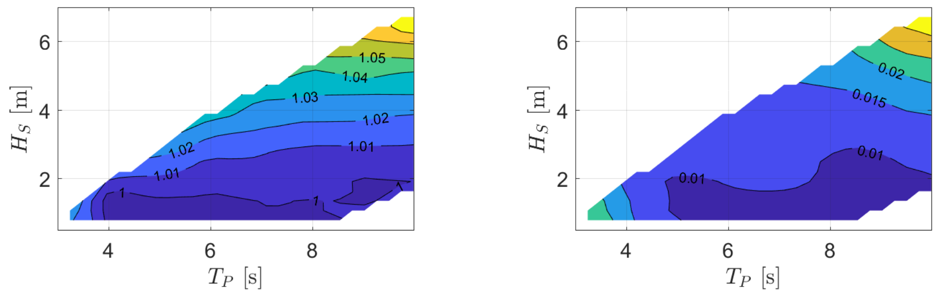

(a) Mean (b) Standard deviation

Figure 12: Wave load effect uncertainty for operational turbine for most likely T_P-values in $4 < V < 25$.

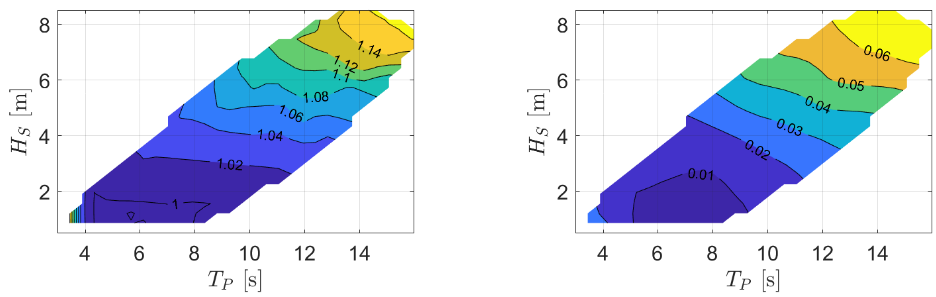

(a) Mean (b) Standard deviation

Figure 13: Wave load effect uncertainty for idling turbine

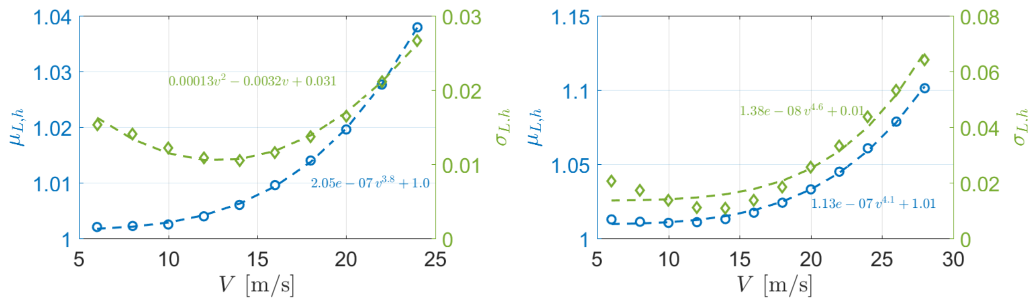

(a) Operational turbine (b) Idling turbine

Figure 14: Wave load effect uncertainty as function of wind speed with fitted curves. Mean value in blue on the left axis and standard deviation in green on the right axis.

The resulting reliability, with and without accounting for the uncertainty in the wave load model, is shown in Fig. 15. A lifetime reduction of approximately 5 years is found when using the second order load model compared to the linear wave load model, indicating a case-specific partial safety factor of approximately 1.2. The second order wave loading results in a more wide-band loading characteristics, increasing the number of high-frequency stress ranges around the natural frequency. Of course, these results would depend on the dynamic properties of the monopile, and is expected to increase for a softer design, i.e. higher natural period for the first vibrational mode.

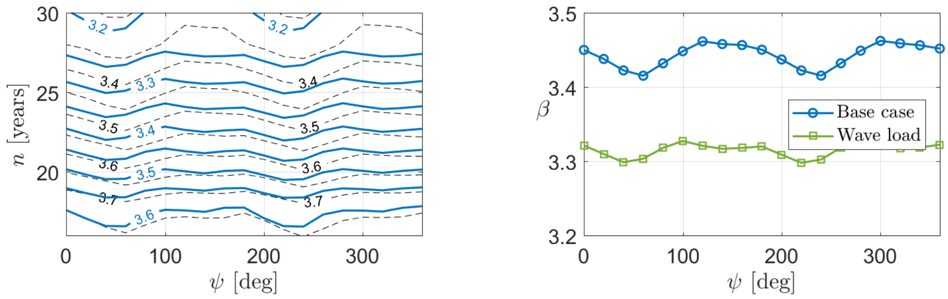

(a) Reliability index as function of years in operation and location on pile. Base case in dashed.

(b) Reliability index for 25 years in operation

Figure 15: Effect of wave load effect uncertainty on the foundation reliability index.

5.5. All combined

In Fig. 16a, all the above uncertainties are accounted for and compared to the base case. By comparing the isoquants for e.g. $\beta = 3.3$, a reduced lifetime of about 10 years is observed, which can be translated to an indicative, case-specific safety factor of $1 + 10/25 = 1.4$. The importance of the wind directional model on the critical fatigue reliability is shown in Fig. 16b, where a significant decrease in the reliability index is observed at $\psi = 60$ and 240 degrees.

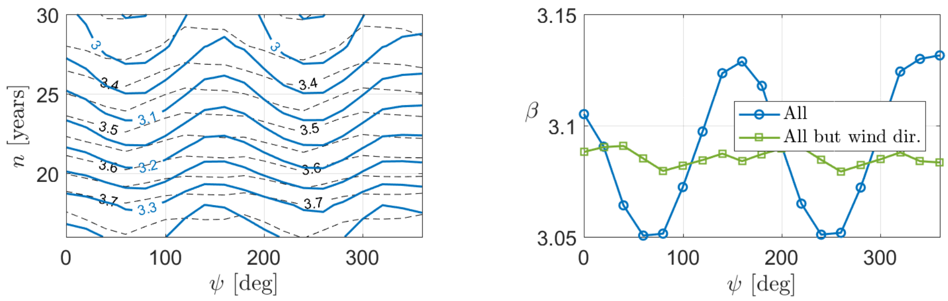

(a) Reliability index as function of years in operation and location on pile. Base case in dashed.

(b) Reliability index for 25 years in operation for all considered uncertainties, with and without wind direction and speed coupling.

Figure 16: Effect of all presented load effect uncertainties on the foundation reliability index.

6. Conclusions

All presented models are believed to represent the reality in a better way than current state-of-the-art models, and all have shown to reduce the structural reliability. It was found that wind-wave misalignment has a significant negative impact on the fatigue life due to dynamic effects. Some indicative, case-specific safety factors that describe the difference between the base case and the higher fidelity case have been found. Although these are only qualitative factors to illustrate the potential over-conservatism, it is clear that the reduced uncertainty in high-fidelity models requires a re-calibration of safety factors in order to be beneficial for the designer. Calibrating new safety factors for bottom-fixed offshore wind turbines may be very elaborate and will require a complete reliability study with time-domain methods like presented in this paper. However, the upside in terms of reduced conservatism will likely justify the investment in computational resources, which easily can be scaled by cloud solutions.

Some limitations in this study include a simplified model for the impact of misalignment of the circumferentially distributed fatigue, and a wave load effect uncertainty independent of the wind-wave misalignment which may be of importance as also noted in [30]. Additionally, the model uncertainty due to soil conditions should be considered in future work, as the soil characteristics may alter the dynamic properties of the system significantly.

Acknowledgement

This work has been carried out at the Centre for Autonomous Marine Operations and Systems (NTNU AMOS). The Norwegian Research Council is acknowledged as the main sponsor of NTNU AMOS. This work was supported by the Research Council of Norway through the Centres of Excellence funding scheme, Project number 223254 - NTNU AMOS.

References

[1] International Electrotechnical Commission, IEC 61400-3, Wind turbinesPart 3: design requirements for offshore wind turbines, Tech. rep. (2009).

[2] DNV GL, Support structures for wind turbines, 2016.

[3] DNV GL, Loads and site conditions for wind turbines, 2016.

[4] J.-T. Horn, J. R. Krokstad, J. Amdahl, Long-Term Fatigue Damage Sensitivity to Wave Directionality in Extra Large Monopile Foundations, Journal of Engineering for the Maritime Environment 232 (2018) 37–49. doi:10.1177/1475090217727136.

[5] S. Schløer, H. Bredmose, H. B. Bingham, The influence of fully nonlinear wave forces on aero-hydro-elastic calculations of monopile wind turbines, Marine Structures 50 (2016) 162–188. doi:10.1016/j.marstruc.2016.06.004.

[6] J. T. Horn, J. R. Krokstad, J. Amdahl, Hydro-Elastic Contributions to Fatigue Damage on a Large Monopile, Energy Procedia 94 (2016) 102–114.

[7] P. Agarwal, L. Manuel, Incorporating irregular nonlinear waves in coupled simulation and reliability studies of offshore wind turbines, Applied Ocean Research 33 (3) (2011) 215–227. doi:10.1016/j.apor.2011.02.001.

[8] M. Moarefzadeh, R. Melchers, Nonlinear wave theory in reliability analysis of offshore structures, Probabilistic Engineering Mechanics 21 (2) (2006) 99–111. doi:10.1016/j.probengmech.2005.04.002.

[9] DNV GL, RP-C203 Fatigue design of offshore steel structures, 2005.

[10] P. Toft-Christensen, Y. Murotsu, Application of Structural Systems Reliability Theory, Springer, 1986.

[11] H. Madsen, S. Krenk, N. Lind, Methods of Structural Safety, Prentice-Hall, Inc., 1986.

[12] J. D. Sørensen, H. S. Toft, Probabilistic Design of Wind Turbines, Energies 3 (2) (2010) 241–257. doi:10.3390/en3020241.

[13] S. Ambühl, F. Ferri, J. P. Kofoed, J. D. Sørensen, Fatigue reliability and calibration of fatigue design factors of wave energy converters, International Journal of Marine Energy 10 (2015) 17–38. doi:10.1016/j.ijome.2015.01.004.

[14] S. Marquez-Dominguez, J. D. Sorensen, Fatigue Reliability and Calibration of Fatigue Design Factors for Offshore Wind Turbines, Energies 5 (6) (2012) 1816–1834. doi:10.3390/en5061816.

[15] M. H. Faber, On the Treatment of Uncertainties and Probabilities in Engineering Decision Analysis, Journal of Offshore Mechanics and Arctic Engineering 127 (3) (2005) 243–248.

[16] M. Paté-Cornell, Uncertainties in risk analysis: Six levels of treatment, Reliability Engineering & System Safety 54 (2) (1996) 95–111. doi:https://doi.org/10.1016/S0951-8320(96)00067-1.

[17] J.-T. Horn, E. M. Bitner-Gregersen, J. R. Krokstad, B. J. Leira, J. Amdahl, A new combination of conditional environmental distributions, Applied Ocean Research 73 (2018) 17–26.

[18] M. Reistad, Ø. Breivik, H. Haakenstad, O. J. Aarnes, B. R. Furevik, J. R. Bidlot, A high-resolution hindcast of wind and waves for the North Sea, the Norwegian Sea, and the Barents Sea, Journal of Geophysical Research: Oceans 116 (5) (2011) 1–18. doi:10.1029/2010JC006402.

[19] C. Bak, F. Zahle, R. Bitsche, A. Yde, L. C. Henriksen, A. Nata, M. H. Hansen, Description of the DTU 10 MW Reference Wind Turbine, Tech. rep., DTU (2013).

[20] E. E. Bachynski, H. Ormberg, Hydrodynamic modeling of large-diameter bottom-fixed offshore wind turbines, in: Proceedings of the ASME 34th International Conference on Ocean, Offshore and Arctic Engineering, ASME, St. Johns, Canada, 2015.

[21] M. H. Hansen, L. C. Henriksen, M. Hartvig, L. Christian, Basic DTU Wind Energy Controller, no. January, 2013.

[22] M. O. L. Hansen, T. Holmås, K. Aas-Jakobsen, J. Amdahl, vpOne - a new FEM based servo-, hydro- and aeroelastic code for wind turbines, in: Offshore Wind Energy, 2009.

[23] S. H. Sørum, J.-T. Horn, J. Amdahl, Comparison of numerical response predictions for a bottom-fixed o ff shore wind turbine, Energy Procedia.

[24] W. Popko, F. Vorpahl, A. Zuga, M. Kohlmeier, J. Jonkman, A. Robertson, T. J. Larsen, A. Yde, K. Saetertrø, K. M. Okstad, J. Nichols, T. A. Nygaard, Z. Gao, D. Manolas, K. Kim, Q. Yu, W. Shi, H. Park, A. Vásquez-Rojas, J. Dubois, D. Kaufer, P. Thomassen, M. J. De Ruiter, T. Van Der Zee, J. M. Peeringa, H. Zhiwen, H. Von Waaden, Offshore Code Comparison Collaboration Continuation (OC4), Phase IResults of Coupled Simulations of an Offshore Wind Turbine with Jacket Support Structure, Journal of Ocean and Wind Energy 1 (1) (2013) 1–11.

[25] N. Kelley, B. Jonkman, Overview of the TurbSim stochastic inflow turbulence simulator, Tech. rep. (2007).

[26] K. Nolte, J. Hansford, Closed-Form Expressions for Determining the Fatigue Damage of Structures Due to Ocean Waves, in: Society of Petroleum Engineers Journal, Vol. 17, 1977, pp. 431–440. doi:10.2118/6250-PA.

[27] E. Ayala-Uraga, T. Moan, Fatigue reliability-based assessment of welded joints applying consistent fracture mechanics formulations, International Journal of Fatigue 29 (3) (2007) 444–456. doi:10.1016/j.ijfatigue.2006.05.010.

[28] H. S. Toft, L. Svenningsen, W. Moser, J. D. Sørensen, M. L. Thøgersen, Assessment of wind turbine structural integrity using response surface methodology, Engineering Structures 106 (2016) 471–483. doi:10.1016/j.engstruct.2015.10.043.

[29] L. Colone, A. Natarajan, N. Dimitrov, Impact of turbulence induced loads and wave kinematic models on fatigue reliability estimates of o ff shore wind turbine monopiles, Ocean Engineering 155 (2018) 295–309. doi:10.1016/j.oceaneng.2018.02.045.

[30] E. Marino, A. Giusti, L. Manuel, Offshore wind turbine fatigue loads: The influence of alternative wave modeling for different turbulent and mean winds, Renewable Energy 102. doi:10.1016/j.renene.2016.10.023.

[31] H. F. Veldkamp, J. van der Tempel, Influence of wave modelling on the prediction of fatigue for offshore wind turbines, Wind Energy 8 (1) (2004) 49–65. doi:10.1002/we.138.

[32] J. Morison, J. Johnson, S. Schaaf, The Force Exerted by Surface Waves on Piles, Journal of Petroleum Technology 2 (05) (1950) 149–154. doi:10.2118/950149-G.

[33] M. B. V. D. Meulen, T. Ashuri, G. J. W. V. Bussel, D. P. Molenaar, Influence of Nonlinear Irregular Waves on the Fatigue Loads of an Offshore Wind Turbine, The Science of Making Torque from Wind

(2012) 1–10doi:10.13140/2.1.3034.5606.

[34] R. C. MacCamy, R. A. Fuchs, Wave Forces on Piles: A Diffraction Theory (1954).

[35] N. Sharma, R. G. Dean, Second-Order Directional Seas and Associated Wave Forces, Society of Petroleum Engineers Journal (February) (1981) 129–140.

[36] J. N. Sharma, R. G. Dean, Contributions to second order directional sea simulation and wave forces, in: Proceedings of the International Conference on Offshore Mechanics and Arctic Engineering - OMAE, Vol. 5, San Diego, CA, 2007, pp. 361–370. doi:10.1115/OMAE2007-29634.

[37] G. Z. Forristall, Wave crest distributions: Observations and second-order theory, Journal of Physical Oceanography 30 (8) (2000) 1931–1943.

[38] R. Eatock Taylor, S. M. Hung, Second order diffraction forces on a vertical cylinder in regular waves., Appl. Ocean Res. 9 (1 , Jan. 1987) (1987) 19–30. doi:10.1016/0141-1187(87)90028-9.

[39] DNV GL, RP-C205 Environmental conditions and environmental loads, Tech. rep. (2017).

[40] M. Tucker, P. Challenor, D. Carter, Numerical simulation of a random sea: a common error and its effect upon wave group statistics, Applied Ocean Research 6 (2) (1984) 118–122. doi:10.1016/0141-1187(84)90050-6.

[41] X. Y. Zheng, T. Moan, S. T. Quek, Numerical simulation of non-Gaussian wave elevation and kinematics based on two-dimensional fourier transform (2006) 1–6.